WIRTSCHAFTS
UNIVERSITÄT
WIEN VIENNA
UNIVERSITY OF
ECONOMICS
AND BUSINESS

MASTER'S THESIS

Option Pricing in the Hypergeometric Volatility Model

submitted by

Simon Mitterhofer BSc

intended degree:

Master of Science (WU) / MSc (WU)

Student ID number: 11910595
Degree programme: Quantitative Finance
Supervisor: Univ.Prof. Dr. Rüdiger Frey

Vienna, September 2025

Abstract

This thesis investigates the Hypergeometric Volatility Model as a flexible framework for option pricing under rough and persistent volatility dynamics. Motivated by empirical evidence of volatility clustering, long memory, and rough sample paths, the model employs a hypergeometric mixing measure to define a latent signal process that drives stochastic volatility. Finite-dimensional approximations enable efficient simulation and practical implementation.

A comprehensive simulation study is conducted to evaluate the model's ability to reproduce key stylized facts of implied volatility surfaces. Five quality criteria are defined, including put-call parity, smile convexity, negative and increasing at-the-money skew, and approximate power-law decay. More than 18,000 parameter constellations are simulated, and the analysis identifies robust parameter regions, particularly roughness indices between 0.10 and 0.25, correlation parameters in $[-0.6, -0.2]$, and moderate volatility scales below 1.4, that consistently generate realistic outcomes.

The model is further validated empirically through calibration to S&P 500 option data. The calibrated surfaces successfully reproduce essential market features, although the best-fit parameters partially deviate from those found optimal in the simulation study. This highlights the trade-off between reproducing stylized facts and achieving close market fit.

Overall, the results demonstrate that the Hypergeometric Volatility Model offers a tractable and empirically consistent framework for modeling option-implied volatility, while also pointing to open challenges in calibration methodology and model robustness.

Acknowledgements

Almost two years have passed since I began my master's in Quantitative Finance, and about one year since this thesis topic was first suggested to me. My academic path started with a bachelor's degree in engineering and led me to this master's, a transition that was at times challenging but ultimately opened up new perspectives and opportunities. This thesis represents the completion of my master's studies and an important milestone in a journey that continues to unfold.

I would like to express my sincere gratitude to Prof. Rüdiger Frey for suggesting this topic, for being an inspiring teacher, and for providing valuable guidance and feedback throughout the process.

I am deeply grateful to my parents, whose constant support has guided me through every decision and path I have taken. I would also like to thank my sister Mara, my brothers Maximilian, Alexander, Elias, and Lukas, and my cousins Armin, Manuel, and Jonas, whose encouragement and presence have made my life joyful and inspiring.

I am equally grateful to my friends from home, to those who accompanied me during my time in Vienna, and to those I got to know during these last two years, all of whom have made this journey memorable and fulfilling.

This journey has been demanding yet rewarding, and I will carry both the knowledge and the memories I have gained as I move forward.

Contents

1 Introduction

The modeling of volatility is a central challenge in modern finance. A good understanding and realistic description of volatility dynamics is essential for accurate derivatives pricing and risk management applications. A common reference is the seminal work by Black and Scholes (1973), which remains one of the most commonly applied mathematical finance papers in practice. In their framework, the asset price is modeled with constant volatility, which allows for an elegant closed-form solution for European option prices. While this approach is mathematically tractable, it does not reflect the dynamics observed in real markets, where volatility is stochastic and exhibits complex time-varying patterns.

Classical extensions of the Black-Scholes model, such as the Heston model (Heston, 1993), account for the stochastic properties and provide greater flexibility. Nevertheless, these models still fail to reproduce important empirical features observed in financial markets. At the time-series level, realized volatility exhibits clustering, long memory, and roughness. Clustering refers to the persistence of high or low volatility periods, while long memory is characterized by slowly decaying autocorrelations over extended time horizons. Roughness, as documented by Gatheral et al. (2018), means that log-volatility follows sample paths that are highly irregular, resembling fractional Brownian motion with a Hurst parameter significantly below 0.5.

At the same time, option market data reveal characteristic patterns in implied volatility surfaces that classical models cannot capture. These include volatility smiles and skews (Rubinstein, 1985), as well as a power-law decay in the at-the-money skew with increasing time to maturity (Gatheral et al., 2018). Since such patterns are structural features of option markets, models that fail to reproduce them systematically misprice options, particularly at short maturities and for deep in- or out-of-the-money strikes.

These empirical shortcomings have motivated the development of rough volatility models, which incorporate highly irregular sample paths, and persistent volatility models, which capture slowly decaying autocorrelations. Recent approaches, such as the Rough Heston model (El Euch and Rosenbaum, 2019) and Brownian semistationary frameworks (Bennedsen et al., 2021), have demonstrated that explicitly accounting for roughness and long memory significantly improves consistency with observed market behavior.

Building on this line of research, Damian (2021) introduced the Hypergeometric Volatility Model. This model employs a hypergeometric mixing measure to define a latent signal process that drives the volatility dynamics. It provides explicit control over both roughness and persistence parameters, offering a unified framework that can capture the main stylized facts of financial markets. Importantly, the model admits computationally tractable finite-dimensional approximations that enable efficient simulation and practical implementation.

This thesis contributes to the literature by conducting a comprehensive simulation-based study of the Hypergeometric Volatility Model. The analysis focuses on the model's ability to reproduce stylized facts of implied volatility surfaces, systematically identifies parameter regions that lead to stable and realistic outcomes, and evaluates the model's empirical performance through calibration to S&P 500 option data. In doing so, the thesis complements the theoretical foundations of the model with extensive numerical analysis and provides practical insights for its implementation.

The structure of the thesis is as follows. Section 2 reviews the literature on volatility stylized facts, limitations of classical models, recent modeling approaches, and simulation techniques. Section 3 introduces the Hypergeometric Volatility Model and describes its mathematical framework. Section 4 presents the simulation methodology for generating option prices and implied volatility surfaces. Section 5 reports comprehensive simulation results and analyzes the influence of model parameters. Section 6 provides empirical validation through calibration to S&P 500 option data. Finally, Section 7 summarizes the findings and discusses their implications for the practical application of rough volatility models.

2 Literature Review

This section reviews key developments in volatility modeling, starting with classical models and their limitations, followed by empirical findings on volatility roughness and persistence. It concludes with modern modeling approaches and practical methods for simulation and approximation.

2.1 Empirical Properties of Volatility and Limitations of Classical Models

Classical models of asset price dynamics typically treat volatility as either a deterministic function of time or a continuous stochastic process driven by standard Brownian motion. The Black-Scholes model (Black and Scholes, 1973) assumes that volatility is constant, while the Heston model (Heston, 1993) introduces stochastic volatility using a mean-reverting square-root process.

Although these models are widely used and mathematically convenient, they do not fully capture how volatility behaves in real financial markets. Volatility tends to cluster, meaning that high or low volatility often persists over time. Realized volatility also exhibits long memory, i.e., past values influence future values over extended periods. These are part of the so-called “stylized facts” of financial time series (Cont, 2001).

In the options market, implied volatility surfaces show patterns that classical models fail to reproduce. These include volatility smiles and skews (Rubinstein, 1985), as well as a power-law decay of the at-the-money (ATM) volatility skew with increasing time to maturity (Gatheral et al., 2018). As a result, option prices from these models often deviate significantly from observed market prices, especially for short maturities or deep in- or out-of-the-money options.

2.2 Motivation for Rough and Persistent Volatility Models

The limitations of classical models have motivated researchers to seek more realistic representations of volatility. Recent empirical evidence indicates that volatility is not only stochastic, but exhibits two key properties that standard models fail to capture: roughness and persistence.

Gatheral et al. (2018) find that realized log-volatility behaves like a fractional Brownian motion with Hurst parameter $H \approx 0.1$. This low Hurst parameter implies highly irregular, or rough, sample paths with negatively correlated increments. This behavior cannot be captured by models driven by standard Brownian motion.

At the same time, volatility exhibits long memory, meaning that its autocorrelations decay slowly over time. This behavior has been documented in Comte and Renault (1998) and further studied in Bennedsen et al. (2021), who develop kernel-based approaches to model long memory.

Further theoretical support comes from Fukasawa (2017), who shows that power-law behavior in the ATM skew can arise under weak regularity conditions on the underlying volatility process. This result suggests that the observed patterns reflect fundamental structural market properties rather than statistical artifacts.

These empirical and theoretical findings have motivated the development of new volatility models that aim to capture both short-term irregularity and long-term memory. Unlike traditional Markovian approaches, these models explicitly incorporate roughness and persistence, leading to improved performance in derivatives pricing and risk management applications.

2.3 Modern Volatility Models

To incorporate roughness and long memory into volatility modeling, several new models have been proposed. These approaches differ in how they capture the time-series properties of volatility and in the extent to which they reproduce key features of implied volatility surfaces.

Gatheral et al. (2018) introduce the Rough Fractional Stochastic Volatility (RFSV) model, where log-volatility follows a fractional Ornstein-Uhlenbeck process driven by fractional Brownian motion with Hurst parameter $H < 0.5$. This specification generates rough sample paths with long-memory characteristics. In option markets, it reproduces the empirically observed power-law decay of the at-the-money skew.

The Rough Heston model by El Euch and Rosenbaum (2019) extends the classical Heston framework by incorporating a fractional kernel in the volatility dynamics. This introduces roughness into the variance process. Although the model is no longer Markovian, it still allows for semi-closed-form characteristic functions, making it suitable for European option pricing.

Other generalizations include affine Volterra processes and affine rough volatility models, such as those in Abi Jaber et al. (2019). Their contribution lies in flexibly capturing memory effects through stochastic convolution equations, while for option pricing they retain affine structures that facilitate tractable computations.

Bennedsen et al. (2021) propose the Brownian semistationary (BSS) framework, which specifies volatility as a convolution integral of Brownian motion with deterministic kernels. This approach provides a flexible structure for modeling the time-series properties of volatility, as the kernel can be adjusted to capture both roughness and persistence.

Extending the convolution-based approach, Damian (2021) introduces the Hypergeometric Volatility Model, which employs a hypergeometric mixing measure to define the convolution kernel. This structure gives explicit control over both short- and long-term dependencies in volatility dynamics. From an option-pricing perspective, the model can generate implied volatility surfaces with realistic skews and smile convexity. The hypergeometric framework serves as the basis for the analysis in this thesis and is presented in detail in Section 3.

2.4 Simulation and Approximation Methods

Rough volatility models often involve infinite-dimensional processes that cannot be simulated exactly, making approximation schemes necessary for practical implementation.

A common approach relies on approximating these processes through mixtures of Ornstein-Uhlenbeck (OU) processes. Carmona and Coutin (1998) show that stochastic convolutions with Laplace-type kernels can be expressed as infinite mixtures of OU processes with varying mean-reversion speeds. This decomposition preserves key properties such as stationarity and mean reversion.

Carmona et al. (2000) propose a finite-dimensional approximation by discretizing the integral over the mixing measure. The result is a weighted sum of OU processes that can be simulated efficiently.

For this spatial discretization, Damian and Frey (2024) suggest the use of a geometric partitioning of the integration domain, ensuring that each of the intervals has the same mass under the mixing

measure. This discretization method is implemented in this thesis for simulating the latent signal process and computing asset price dynamics under the Hypergeometric Volatility Model.

3 Modeling Framework

This section presents the mathematical framework of the Hypergeometric Volatility Model. The model describes a risk-neutral asset price process with stochastic volatility driven by a latent signal process. The volatility dynamics are designed to capture both roughness and long memory. The framework is developed by first specifying the asset price and volatility model, then introducing the signal process, and finally describing its approximation and normalization.

3.1 Asset Price and Volatility Model

Consider a financial market with a constant risk-free interest rate $r > 0$ and a non-dividend-paying risky asset S. The asset price is modeled as a stochastic process $S = \{S_t\}_{0 \le t \le T}$. Under the risk-neutral measure, its dynamics are given by the stochastic differential equation

$$\mathrm{d}S_t = rS_t\,\mathrm{d}t + \lambda(X_t)S_t\,\mathrm{d}W_t, \tag{1}$$

where W is a standard Brownian motion and $\lambda(X_t)$ denotes the stochastic volatility process.

Following Bennedsen et al. (2021), the volatility is modeled as an exponential function of a latent signal process $X = \{X_t\}_{0 \le t \le T}$:

$$\lambda(X_t) = b \cdot \exp\left(a \cdot \frac{X_t}{\bar{\sigma}_X} - \frac{a^2}{2}\right), \tag{2}$$

where $b > 0$ is the base volatility level and $a > 0$ is a volatility scale parameter. The term $\bar{\sigma}_X$ denotes the long-term standard deviation of the signal and serves as a normalization factor. The correction term $-a^2/2$ centers the volatility level, so that $\mathbb{E}[\lambda(X_t)] \approx b$ under the stationary distribution of X_t.

This specification ensures strictly positive volatility and allows for occasional large spikes. The parameters a and b separately control the volatility's fluctuation scale and long-term level.

3.2 Signal Process

The latent signal process X introduces roughness and persistence into the volatility dynamics. It is defined as a stochastic Volterra process (Abi Jaber et al., 2019) of the form

$$X_t = \int_0^t h(t-s)\,\mathrm{d}B_s, \tag{3}$$

where B is a standard Brownian motion and $h : \mathbb{R}_+ \to \mathbb{R}$ is a deterministic kernel function.

The kernel h is specified as the Laplace transform of a non-negative mixing measure μ:

$$h(u) = \int_0^\infty e^{-xu}\mu(x)\,\mathrm{d}x, \tag{4}$$

$$\mu(x) = (1+x)^{-\gamma_1}x^{-\gamma_2}, \quad \gamma_1, \gamma_2 > 0. \tag{5}$$

For the process to exhibit well-defined roughness and persistence properties, the parameters must satisfy the restrictions

$$\gamma_2 < \tfrac{1}{2}, \qquad \tfrac{1}{2} < \gamma_1 + \gamma_2 < 1. \tag{6}$$

The parameters γ_1 and γ_2 jointly control the short- and long-term behavior of the kernel. Larger values of γ_2 increase persistence, while for fixed γ_2, smaller values of γ_1 correspond to greater roughness. The formal link between these parameters and the Hurst index is derived in Section 3.3.

As shown in Carmona and Coutin (1998), stochastic convolutions with Laplace-type kernels can be represented as infinite mixtures of Ornstein-Uhlenbeck (OU) processes. By Fubini's theorem, the signal process can be rewritten as

$$X_t = \int_0^\infty Z_t^{(x)} \mu(x)\,\mathrm{d}x, \qquad Z_t^{(x)} := \int_0^t e^{-x(t-s)}\,\mathrm{d}B_s, \tag{7}$$

where each $Z_t^{(x)}$ is an OU process with mean-reversion speed x driven by the common Brownian motion B.

3.3 Roughness and Long Memory

The small- and large-time behavior of the kernel $h(u)$ determines the roughness and persistence of the signal process X. Following the derivation in Damian (2021), and using the substitution $y = xu$, the kernel admits the asymptotic behavior

$$h(u) \sim u^{\gamma_1+\gamma_2-1}, \quad u \to 0, \tag{8}$$

$$h(u) \sim u^{\gamma_2-1}, \quad u \to \infty. \tag{9}$$

Based on these asymptotics, the path properties of X can be characterized using the results of Bennedsen et al. (2021). Proposition 2.1 in their paper shows that the process exhibits rough paths if its Hurst index

$$H := \gamma_1 + \gamma_2 - \tfrac{1}{2} \tag{10}$$

satisfies $0 < H < \frac{1}{2}$. In this case, the sample paths are rougher than standard Brownian motion.

Similarly, Proposition 2.2 establishes that the process exhibits long memory if $0 < \gamma_2 < \frac{1}{2}$, since the kernel $h(u)$ then decays slowly as $u \to \infty$. This condition is precisely the one imposed on the parameter range in Section 3.2. Together, these results provide the formal link between the parameterization of the hypergeometric kernel and the roughness and persistence properties of the signal process.

3.4 Finite-Dimensional Approximation

The infinite-dimensional representation in (7) is approximated by a finite sum of J OU processes. Following Carmona et al. (2000), the signal is approximated by

$$X_t^{(J)} = \sum_{j=1}^{J} c_j Z_t^{(j)}, \tag{11}$$

where each $Z_t^{(j)}$ solves the SDE

$$\mathrm{d}Z_t^{(j)} = -\kappa_j Z_t^{(j)}\,\mathrm{d}t + \mathrm{d}B_t, \quad Z_0^{(j)} = 0. \tag{12}$$

The weights c_j and mean-reversion rates κ_j are computed from a partition of the positive real line:

$$c_j = \int_{\xi_{j-1}}^{\xi_j} \mu(x)\,\mathrm{d}x, \tag{13}$$

$$\kappa_j = \frac{\int_{\xi_{j-1}}^{\xi_j} x\mu(x)\,\mathrm{d}x}{\int_{\xi_{j-1}}^{\xi_j} \mu(x)\,\mathrm{d}x}. \tag{14}$$

This representation makes the process $X_t^{(J)}$ Markovian in $\mathbb{R}^J$, enabling efficient simulation.

To construct the partition $0 < \xi_0 < \xi_1 < \cdots < \xi_J < \infty$, Damian and Frey (2024) propose a geometric scheme:

$$\xi_0 = J^{-2\alpha}, \quad \xi_J = J^{4-2\alpha}, \tag{15}$$

$$q = \left(\frac{\xi_J}{\xi_0}\right)^{1/J}, \quad \text{so that } \xi_j = \xi_0 q^j, \tag{16}$$

where $\alpha = H + \frac{1}{2}$ is related to the process roughness. This choice ensures that each partition interval $[\xi_{j-1}, \xi_j]$ contains equal mass under the mixing measure μ.

3.5 Long-Term Variance

To normalize the volatility in (2), the long-term variance of the signal process is computed. Since X_t is centered, its variance is

$$\mathrm{Var}[X_t] = \int_0^t h^2(u)\,\mathrm{d}u = \iint_{(0,\infty)^2} \frac{1 - e^{-(x+y)t}}{x+y}\mu(x)\mu(y)\,\mathrm{d}x\,\mathrm{d}y. \tag{17}$$

As $t \to \infty$, the process becomes stationary with limiting variance

$$\bar{\sigma}_X^2 := \lim_{t\to\infty} \mathrm{Var}[X_t] = \iint_{(0,\infty)^2} \frac{1}{x+y}\mu(x)\mu(y)\,\mathrm{d}x\,\mathrm{d}y. \tag{18}$$

In the finite-dimensional case, the long-term variance of $X_t^{(J)}$ is

$$\bar{\sigma}_{X,J}^2 := \lim_{t\to\infty} \mathrm{Var}\left[\sum_{j=1}^J c_j Z_t^{(j)}\right] = \sum_{i=1}^J \sum_{j=1}^J \frac{c_i c_j}{\kappa_i + \kappa_j}. \tag{19}$$

This variance is used to normalize the signal in (2), ensuring comparability across parameter choices and discretization levels.

4 Simulation Methodology

This section provides a detailed description of the simulation framework used to generate asset price paths under the Hypergeometric Volatility Model. First, the latent volatility signal is simulated. Then, the asset price dynamics are determined by sampling the log-returns based on the generated volatility. Finally, European option prices are computed via Monte Carlo simulation, and implied volatilities are derived through inversion of the Black-Scholes formula.

4.1 Time Discretization

The model presented in Section 3 is defined in continuous time. However, for the purpose of simulation, a discrete-time version is considered. Let T denote the time horizon and define an equidistant time grid $0 = t_0 < t_1 < \ldots < t_N = T$ with step size $\Delta t = T/N$. At each time step t_i for $i = 0, \ldots, N-1$, Brownian motion increments are generated, and then the state of the signal and asset price processes are updated.

The simulation requires two Brownian motions: B, which drives the volatility signal, and W, which drives the asset price. These are modeled as correlated processes to reflect the leverage effect commonly observed in financial markets. At each time step t_i, correlated Brownian motion increments $(\Delta B_i, \Delta W_i)$ are generated such that $\mathrm{Cov}(\Delta B_{t_i}, \Delta W_{t_i}) = \rho \cdot \Delta t$.

This is achieved by drawing two independent standard normal random variables ε_i and η_i at each time step. Then the discrete Brownian increments are

$$\Delta B_{t_i} = \sqrt{\Delta t} \cdot \varepsilon_i, \tag{20}$$

$$\Delta W_{t_i} = \rho \cdot \Delta B_{t_i} + \sqrt{1-\rho^2} \cdot \sqrt{\Delta t} \cdot \eta_i. \tag{21}$$

This is repeated at each of the N time points.

4.2 Simulation of the Signal Process

The latent volatility signal is modeled as a finite-dimensional approximation of an infinite mixture of Ornstein-Uhlenbeck processes, as described in Section 3.4. For simulation purposes, the explicit solution of the Ornstein-Uhlenbeck stochastic differential equation is used. This method ensures numerical stability and avoids discretization bias.

Let J denote the number of Ornstein-Uhlenbeck components, with mean-reversion speeds κ_j and weights c_j obtained from the geometric partitioning scheme. For each component $Z_t^{(j)}$, the update rule is given by

$$Z_{t_{i+1}}^{(j)} = e^{-\kappa_j \Delta t} Z_{t_i}^{(j)} + \sqrt{\frac{1 - e^{-2\kappa_j \Delta t}}{2\kappa_j}} \cdot \frac{\Delta B_t}{\sqrt{\Delta t}}, \tag{22}$$

where ΔB_t corresponds to the volatility-driving Brownian motion across all $j = 1, \ldots, J$.

After updating all $Z^{(j)}$, the signal process is computed at each time step as a linear combination:

$$X_{t_i}^{(J)} = \sum_{j=1}^{J} c_j Z_{t_i}^{(j)}. \tag{23}$$

4.3 Volatility Specification

Once the signal process X_t has been generated, the stochastic volatility process is obtained through the exponential transformation

$$\lambda(X_{t_i}) = b \cdot \exp\left(a \cdot \frac{X_{t_i}}{\bar{\sigma}_X} - \frac{a^2}{2}\right), \tag{24}$$

where $b > 0$ controls the volatility level and $a > 0$ determines the sensitivity to changes in the signal. This specification ensures that the volatility remains strictly positive and allows for extreme spikes, in line with empirical observations in financial markets. To ensure comparability across different parameter settings, the signal is normalized by its long-term standard deviation $\bar{\sigma}_X$ and centered by the correction term, as discussed in Section 3.5.

The entire volatility path $\lambda(X_{t_i})_{i=0}^N$ is computed prior to asset price simulation and stored for later use in simulating the asset price process.

4.4 Simulation of the Asset Price Process

Given the discrete-time volatility path and the correlated Brownian motion increments from Equations (20)-(21), the asset price process is simulated using a log-Euler scheme under the risk-neutral measure. The log-return over each time step is given by

$$\log\left(\frac{S_{t_{i+1}}}{S_{t_i}}\right) = \left(r - \frac{1}{2}\lambda(X_{t_i})^2\right)\Delta t + \lambda(X_{t_i}) \cdot \Delta W_{t_i}, \tag{25}$$

where r denotes the constant risk-free interest rate. This recursion ensures that the asset price remains strictly positive and reflects the impact of the stochastic volatility.

To compute the entire path of the asset price process, log-returns are accumulated as follows

$$\log S_{t_{i+1}} = \log S_{t_i} + \left(r - \frac{1}{2}\lambda(X_{t_i})^2\right)\Delta t + \lambda(X_{t_i}) \cdot \Delta W_{t_i}, \tag{26}$$

starting from an initial price $S_0 > 0$. The final price path is then recovered by exponentiating the log-values.

This procedure results in a full discrete-time asset price path $S_0, S_1, \ldots, S_N$. The simulation guarantees that the asset price remains strictly positive at all times.

4.5 Monte Carlo Option Pricing

The simulated asset price paths are used to compute European option prices via risk-neutral Monte Carlo valuation. Let M denote the number of independent Monte Carlo paths. For each simulation run $m = 1, \ldots, M$, the price points corresponding to a pre-specified set of maturities $\{T_1, \ldots, T_Q\} \subset \{t_0, \ldots, t_N\}$ are extracted from the full trajectory $\{S_{t_i}^{(m)}\}_{i=0}^N$. This allows for efficient pricing of European options across multiple maturities without resimulating asset paths.

For each maturity T_q and strike K_l from the predefined grid $\{K_1, \ldots, K_L\}$, the discounted expected

payoff of a European call option is estimated as

$$C(K_l, T_q) = \mathbb{E}\left[e^{-rT_q}(S_{T_q} - K_l)^+\right] \approx \frac{e^{-rT_q}}{M} \sum_{m=1}^{M} \max\left(S_{T_q}^{(m)} - K_l, 0\right), \tag{27}$$

and analogously, the European put price is given by

$$P(K_l, T_q) = \mathbb{E}\left[e^{-rT_q}(K_l - S_{T_q})^+\right] \approx \frac{e^{-rT_q}}{M} \sum_{m=1}^{M} \max\left(K_l - S_{T_q}^{(m)}, 0\right). \tag{28}$$

This procedure yields a matrix of option prices for each combination of strike and maturity. All pricing is performed under the risk-neutral measure, using the constant risk-free rate r for discounting.

4.6 Implied Volatility Surface Computation

For each computed option price, the corresponding implied volatility is obtained by inverting the Black-Scholes pricing formula. Let V_{MC} denote the Monte Carlo price of a call or put option with strike K and maturity T. The implied volatility σ_{IV} is defined as the unique positive solution to

$$V_{\text{BS}}(K, T; \sigma_{\text{IV}}) = V_{\text{MC}}, \tag{29}$$

where V_{BS} denotes the Black-Scholes price given the same K, T, r, and S_0.

The inversion is carried out numerically using a root-finding algorithm, such as the bisection method, with appropriate upper and lower bounds, and convergence tolerance. To ensure robustness, option values that are near zero or very deep in-the-money are excluded from inversion, as they may lead to numerical instability.

To obtain a well-behaved implied volatility surface, missing entries in the volatility matrix are interpolated along the maturity dimension, with short gaps of consecutive missing values filled by linear interpolation. In addition, empirically unrealistic regions of the strike-maturity grid, corresponding to very short maturities combined with extreme levels of moneyness where no options are typically traded, are systematically excluded. This procedure ensures that the resulting surface is continuous in its central region while remaining consistent with observed market characteristics at the boundaries.

The result is a matrix of implied volatilities $\sigma_{\text{IV}}(K_l, T_q)$ that forms the simulated volatility surface. This surface serves as the primary output of the model and forms the basis for the analysis in Section 5.

4.7 Output for Subsequent Analysis

Each complete simulation run with M Monte Carlo paths and fixed model parameters is referred to as a scenario. A scenario is fully characterized by a specific configuration of the parameters $(H, \gamma_2, \rho, a, b, r, J)$. The roughness parameter H is used in place of γ_1, which governs the short-term kernel behavior, since both are linked through the relation $H = \gamma_1 + \gamma_2 - \frac{1}{2}$ (see Equation (10)).

The simulation of a scenario produces three main output components derived from the generated asset price paths and subsequent option pricing.

First, two matrices of option values are computed: one for European call options and one for European put options. These matrices are evaluated over a common pre-defined grid of strikes $\{K_1, \ldots, K_L\}$ and maturities $\{T_1, \ldots, T_Q\}$. Both are retained to allow for consistency checks, such as verification of put-call parity.

Second, the option prices are transformed into implied volatilities via numerical inversion of the Black-Scholes formula, as described in Section 4.6. This yields two implied volatility matrices, one for calls and one for puts. These are then aggregated by computing the elementwise average wherever both values are available. If only one value is available due to numerical issues, it is used directly.

Finally, the aggregated implied volatility surface is retained as the main object of interest. It provides the basis for evaluating the quality criteria and conducting the analyses in Section 5.

In summary, the simulation of a scenario delivers:

- The parameter configuration $(H, \gamma_2, \rho, a, b, r, J)$,
- Two option value matrices (calls and puts), primarily for diagnostic purposes,
- One aggregated implied volatility matrix, used for subsequent analysis.

All matrices are computed on the same strikes-maturities grid. The aggregated implied volatility surface is the central output used in the simulation study.

5 Simulation Results and Analysis

This section presents the analysis of the simulation results. A simulated scenario is considered successful if the resulting implied volatility surface satisfies all five quality criteria introduced in Section 5.1. These criteria are motivated by empirical stylized facts observed in financial markets and are designed to assess whether a simulated surface can be regarded as realistic.

First, the quality criteria are formally defined. Next, a ceteris paribus analysis is conducted to isolate the effect of individual model parameters. Finally, the simulation output is evaluated across a broad set of parameter constellations, and parameter ranges with high success rates are identified.

5.1 Simulation Quality Criteria

Based on empirical observations in financial markets, five quality criteria are defined to assess the plausibility of simulated implied volatility surfaces:

- Put-call parity must hold.
- The implied volatility smile must exhibit convexity.
- The at-the-money (ATM) volatility skew should be negative.
- The ATM skew should increase with time to maturity.
- The ATM skew term structure should decay approximately according to a power law.

A simulation scenario is considered successful if the resulting implied volatility surface satisfies all five quality criteria.

Put-Call Parity Criterion

The put-call parity (see Björk, 2009) establishes a fundamental no-arbitrage relationship between the prices of European call and put options. At time t, it states:

$$C_t - P_t = S_t - K \cdot B(t,T), \tag{30}$$

where C_t and P_t denote the prices of a European call and put option with strike K and maturity $T \geq t$, S_t is the spot price of the underlying asset, and $B(t,T) = e^{-r(T-t)}$ is the discount factor under a constant risk-free rate r.

In the simulation, this relation is evaluated at $t = 0$. The element-wise relative deviation from parity is computed as:

$$\text{Relative Error}_{l,q} = \left| \frac{C_0^{(l,q)} - P_0^{(l,q)} - \left(S_0 - K_l e^{-rT_q}\right)}{S_0} \right|, \tag{31}$$

where the indices (l,q) refer to strike K_l and maturity T_q.

The criterion is satisfied if the mean relative deviation across all (l,q) does not exceed 0.1% and the maximum deviation does not exceed 0.5%. Meeting this condition ensures internal consistency between simulated call and put prices, allowing them to be aggregated into a single implied volatility surface.

Smile Convexity Criterion

In financial markets, implied volatility typically exhibits a smile-shaped pattern across strikes for a fixed maturity: it tends to be lowest at-the-money and higher for deep in- or out-of-the-money options. To assess convexity, a quadratic polynomial is fitted to the implied volatilities for each maturity.

The criterion is satisfied if the fitted parabola has a positive leading coefficient and an R^2 value above 90%. This convex smile pattern must be observed for the shortest maturity and for at least 90% of all maturities overall.

ATM Skew Negativity Criterion

Empirically, the ATM volatility skew tends to be negative, meaning that implied volatility decreases with increasing moneyness around the at-the-money level. The ATM skew is defined as in Bayer et al. (2016) by

$$\psi(\tau) := \frac{\partial}{\partial k}\sigma_{\mathsf{BS}}(k,\tau)\Big|_{k=0}, \tag{32}$$

where $\sigma_{\mathsf{BS}}(k,\tau)$ is the implied Black-Scholes volatility for log-moneyness k and maturity τ.

The criterion is satisfied if $\psi(\tau) < 0$ for at least 90% of the maturities.

ATM Skew Increase Criterion

It is commonly observed that the magnitude of the ATM skew diminishes with increasing maturity, resulting in a flatter term structure. Hence, the ATM skew function $\psi(\tau)$ is expected to increase with maturity, i.e., become less steep for longer maturities.

The criterion is satisfied if a linear regression of $\psi(\tau)$ against maturity yields a positive slope.

ATM Skew Power Law Criterion

Empirical studies suggest that the ATM skew decays approximately as a power law (see Fukasawa, 2011 and Gatheral et al., 2018) of the form:

$$\psi(\tau) \sim \tau^{-\gamma}, \tag{33}$$

with $\gamma = \frac{1}{2} - H$. The criterion is satisfied if a linear regression on the log-log plot of $\psi(\tau)$ versus τ achieves an R^2 value greater than 90%.

5.2 Effects of Individual Parameters

This section analyzes how varying one model parameter, while keeping all others fixed, affects the shape of the implied volatility surface and the performance with respect to the simulation quality criteria. The analysis is conducted in a ceteris paribus fashion and provides intuition for the results of the full parameter sweep presented in later sections.

Effect of the Roughness Parameter H

For lower values of H (i.e., rougher sample paths), the short-term ATM skew decreases in magnitude. Additionally, the slope of the log-log regression fitted to the ATM skew term structure flattens, indicating that the power-law exponent decreases in absolute value as H decreases.

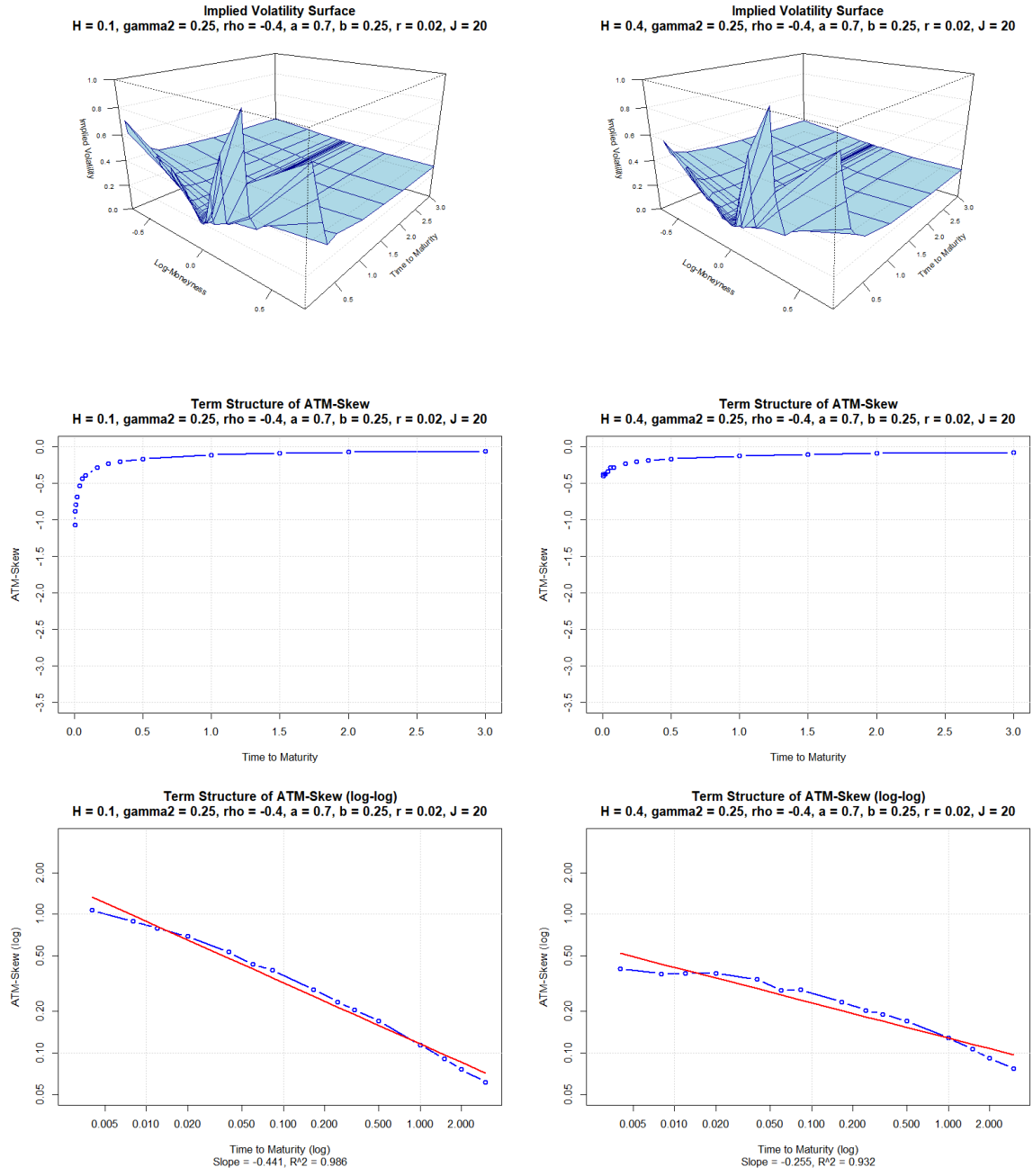

Figure 1: Effect of roughness index H on the implied volatility surface. Left: $H = 0.10$. Right: $H = 0.40$.

Effect of Persistence Parameter γ_2

Higher values of γ_2 increase the persistence in the signal process. This reduces the short-term ATM skew and flattens the power-law slope in the log-log skew regression. Overall, increased persistence slightly lowers the implied volatility surface, especially at short maturities.

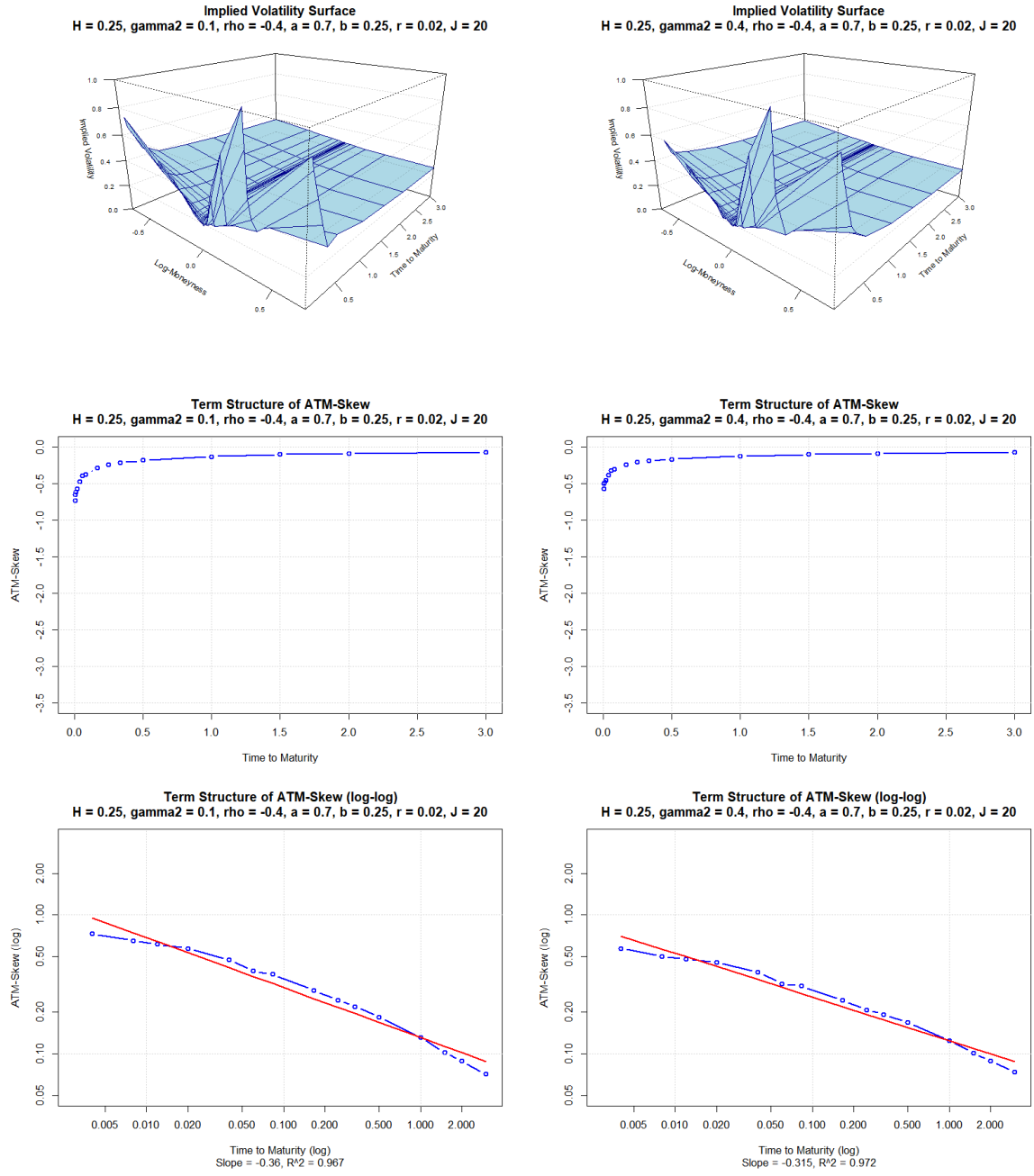

Figure 2: Effect of persistence parameter γ_2 on the implied volatility surface. Left: $\gamma_2 = 0.10$. Right: $\gamma_2 = 0.40$.

Effect of Correlation Parameter ρ

Increasing the correlation ρ between the Brownian motions driving the asset price and the volatility process (i.e., reducing the leverage effect) tilts the implied volatility surface to the left. This results in lower implied volatilities for positive log-moneyness and higher volatilities for negative log-moneyness. As a consequence, the magnitude of the ATM skew increases.

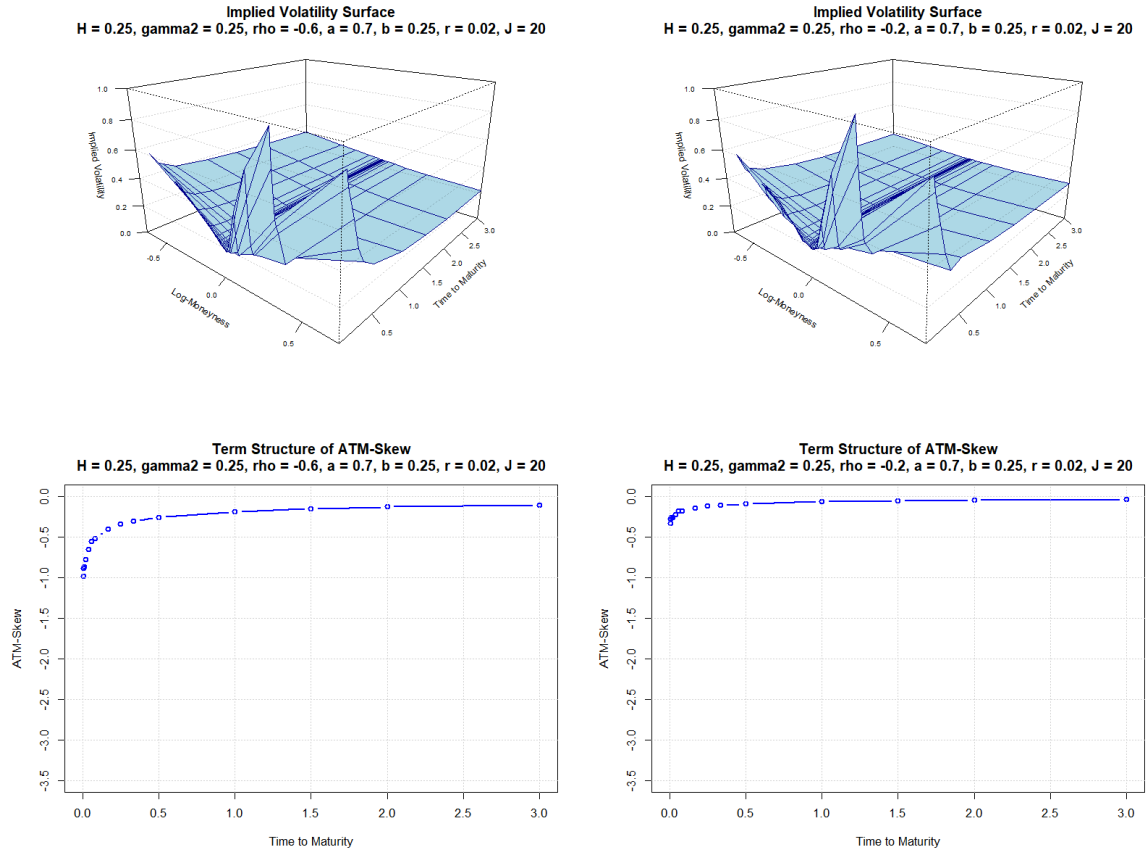

Figure 3: Effect of correlation ρ on the implied volatility surface. Left: $\rho = -0.6$. Right: $\rho = -0.2$.

Effect of Volatility Scale Parameter a

Increasing the volatility scale parameter a amplifies the influence of the latent signal process on the volatility level. This leads to higher implied volatilities in the wings, i.e., for deep in- or out-of-the-money options. The ATM skew magnitude also increases, particularly for short maturities.

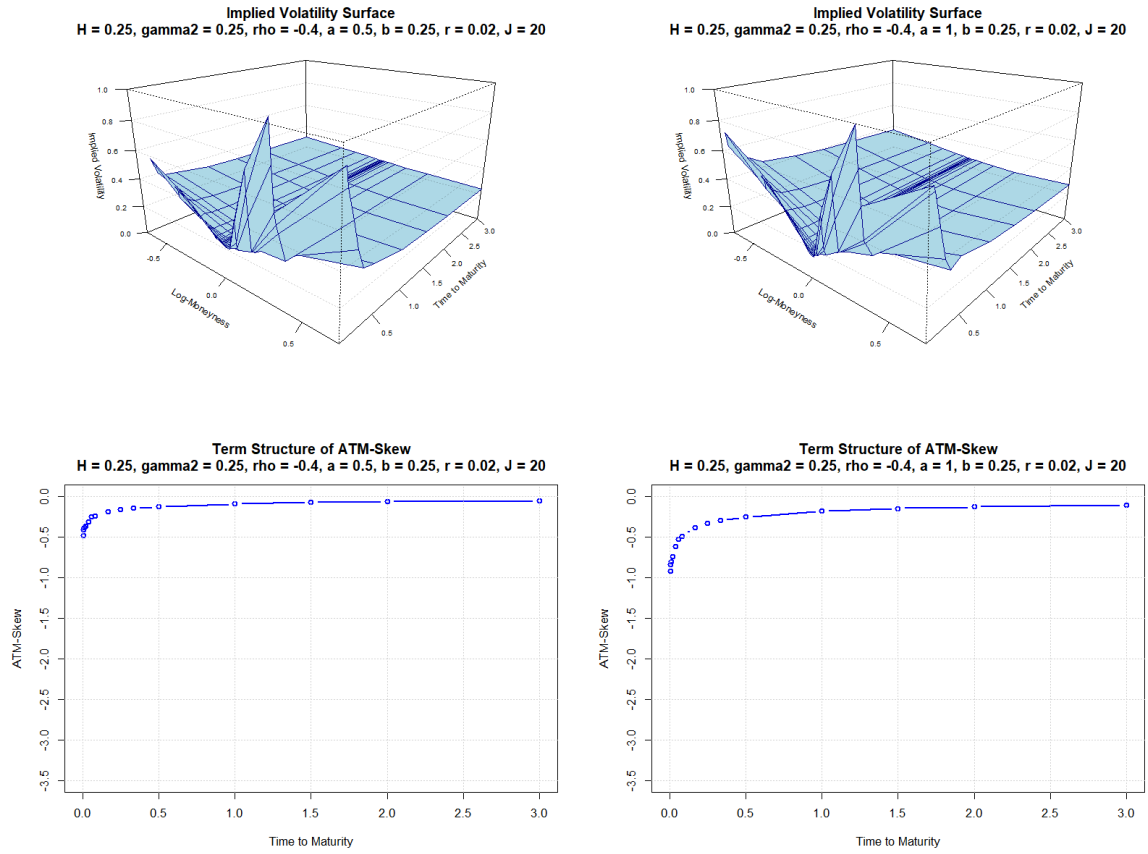

Figure 4: Effect of volatility scale parameter a on the implied volatility surface. Left: $a = 0.5$. Right: $a = 1.0$.

Effect of Base Volatility Level b

Raising the base volatility level b shifts the entire implied volatility surface upward. Additionally, it increases the magnitude of the slope in the log-log regression of the ATM skew, suggesting a steeper power-law decay and hence a stronger term-structure effect in the skew.

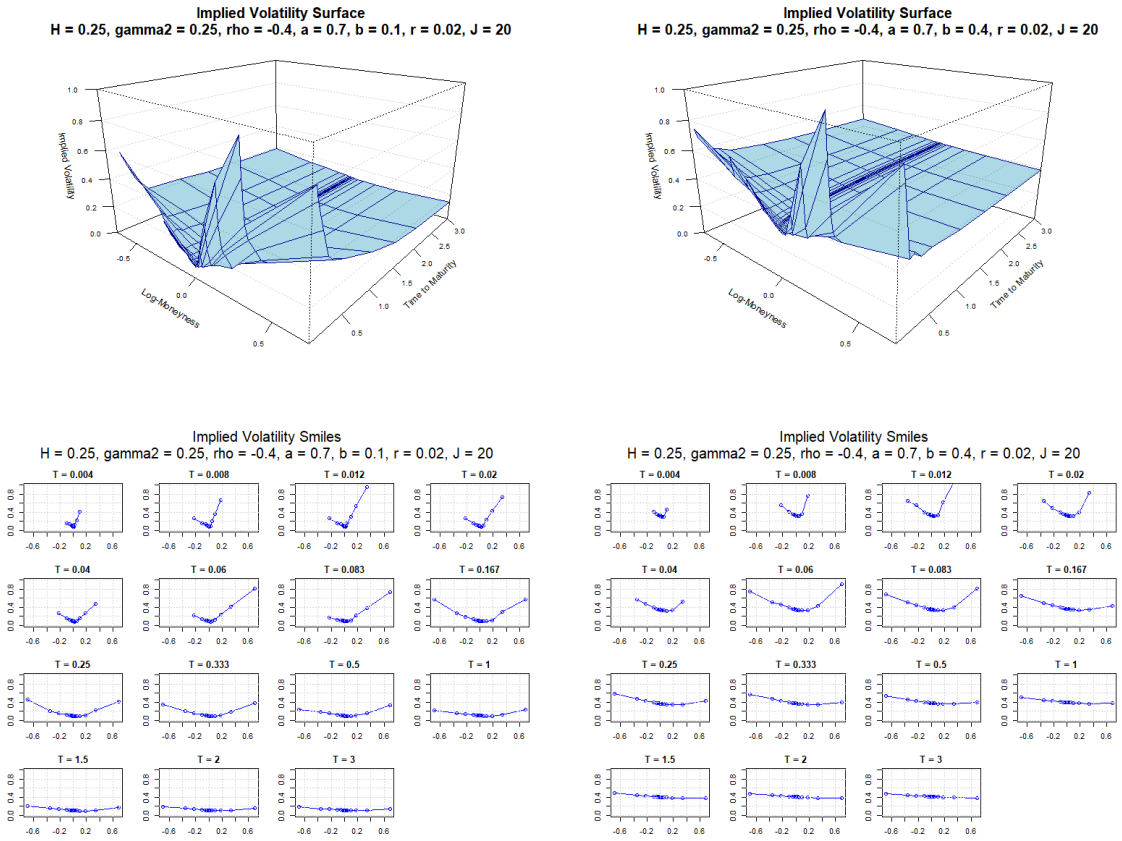

Figure 5: Effect of base volatility level b on the implied volatility surface. Left: $b = 0.1$. Right: $b = 0.4$.

Effect of Risk-Free Interest Rate r

Changes in the risk-free interest rate r have no effect on the implied volatility surface, as expected under risk-neutral pricing. This serves as a consistency check for the numerical implementation.

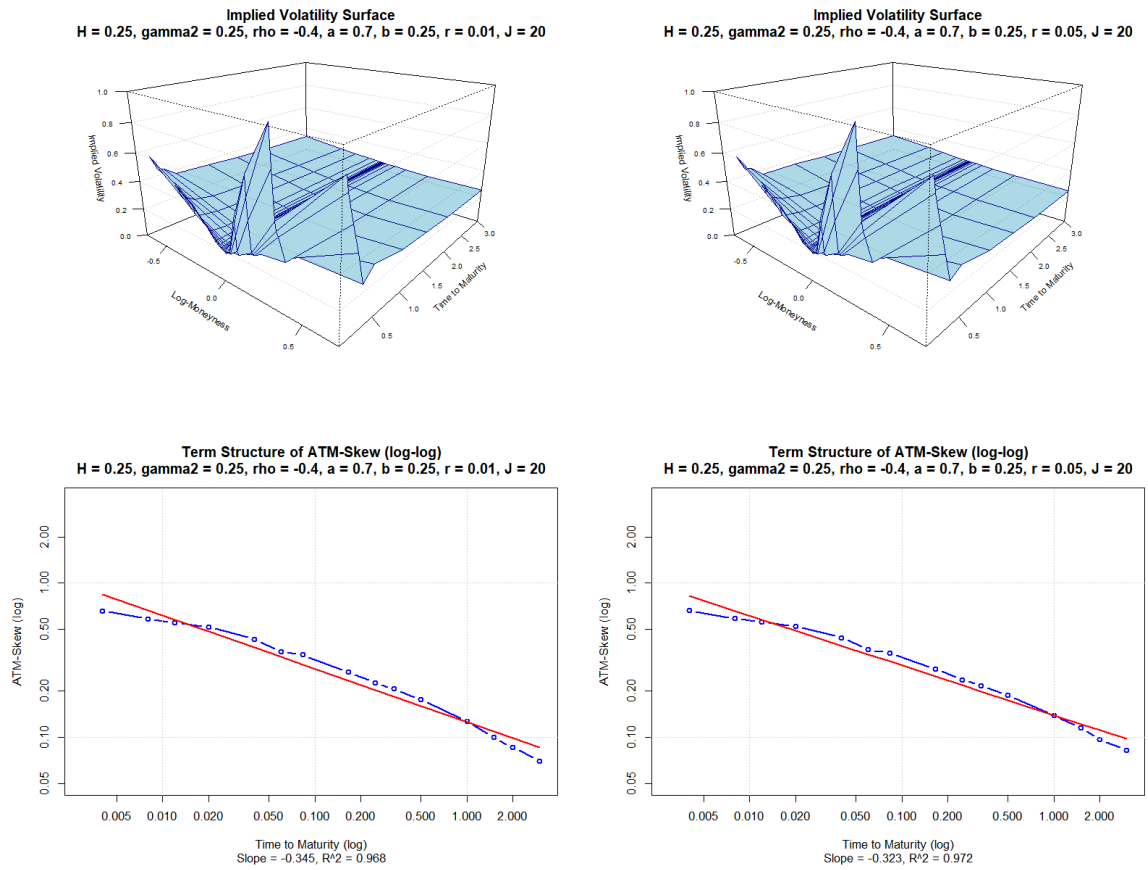

Figure 6: Effect of risk-free interest rate r on the implied volatility surface. Left: $r = 0.01$. Right: $r = 0.05$.

Effect of Approximation Parameter J

The stability of the simulation depends on the level of approximation of the signal process. As J increases, the at-the-money (ATM) skew becomes more pronounced, indicating that a finer approximation of the rough volatility process allows the power-law behavior of the ATM skew term structure to emerge more clearly, particularly for very short maturities.

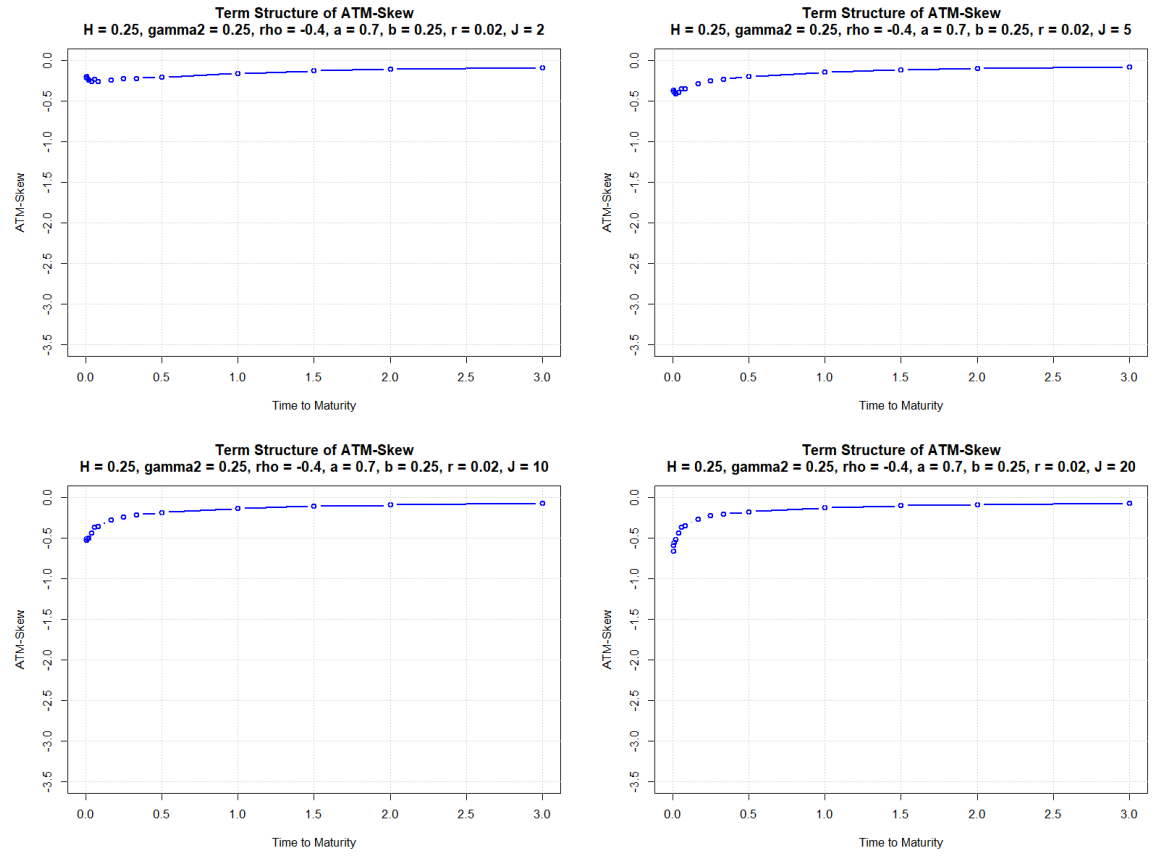

Figure 7: Effect of approximation parameter J on the ATM implied volatility skew. Top-left to bottom-right: $J = 2, 5, 10, 20$.

5.3 Success Rate Analysis

To evaluate model performance, this section analyzes the proportion of simulation scenarios that satisfy the five quality criteria defined in Section 5.1. Each scenario corresponds to a unique configuration of model parameters, and is simulated using 100,000 Monte Carlo paths to generate the asset price dynamics required for option pricing. A scenario is considered successful if all five criteria are met.

Parameter Grid Used in the Simulation Study

The simulation study was based on a broad parameter grid chosen to reflect realistic variation in volatility dynamics. In total, 18,225 scenarios were evaluated with the following parameter values:

- Roughness index $H \in \{0.05, 0.10, 0.15, 0.20, 0.25, 0.30, 0.35, 0.40, 0.45\}$
- Persistence parameter $\gamma_2 \in \{0.05, 0.10, 0.15, 0.20, 0.25, 0.30, 0.35, 0.40, 0.45\}$
- Correlation $\rho \in \{-0.8, -0.7, -0.6, -0.5, -0.4, -0.3, -0.2, -0.1, 0\}$
- Volatility scale parameter $a \in \{0.5, 0.7, 1.0, 1.4, 2.0\}$
- Base volatility level $b \in \{0.10, 0.15, 0.20, 0.25, 0.30\}$

The risk-free rate r and the approximation parameter J are kept constant at $r = 0.02$ and $J = 20$. The short-term parameter γ_1 was computed as $\gamma_1 = H + \frac{1}{2} - \gamma_2$ according to Equation (10), ensuring the correct asymptotic behavior of the hypergeometric kernel.

Overall Success Rates

Put-call parity is satisfied in 93% of simulations, smile convexity in 66%, skew negativity in 99%, skew increase in 96%, and the power-law fit in 70%. All five criteria are met simultaneously in 54% of scenarios. Table 1 summarizes the results.

Criterion	Put-Call Parity	Smile Convexity	Skew Negative	Skew Increasing	Skew Power Law
Success Rate	93%	66%	99%	96%	70%

Table 1: Overall success rates across all simulation scenarios.

Put-call parity success drops for high a and improves with higher H, higher γ_2, lower ρ, and lower b. Smile convexity worsens for lower ρ and high a, peaks for $H \in [0.10, 0.15]$ and larger b, and is unaffected by γ_2. Skew negativity is always satisfied when $\rho < 0$. Skew increase benefits from low H and is otherwise met for all negative correlations. The power-law fit improves for low H, low ρ, and high b, but drops sharply at $a = 2$ (optimal at $a = 1$).

Effect of the Roughness Parameter H

The roughness index H strongly influences results. Put-call parity rises from 84% at $H = 0.05$ to 99% at $H = 0.45$. Smile convexity is highest for $H \in [0.10, 0.25]$ (69-71%) but falls to 58% at $H = 0.45$. Skew negativity remains above 99% throughout. Skew increase declines from 100% at $H \leq 0.15$ to

90% at $H = 0.45$. The power-law fit rate falls from 77% at $H = 0.05$ to 57% at $H = 0.45$. Overall, $H \in [0.10, 0.25]$ offers the best trade-off.

Effect of the Persistence Parameter γ_2

The persistence parameter γ_2 has little effect. Put-call parity improves from 90% to 96% as γ_2 increases, while smile convexity drops slightly (67% to 64%). Skew negativity stays at 99% throughout, skew increase declines marginally, and the power-law fit remains near 70%. Slightly better overall results occur for $\gamma_2 \in [0.05, 0.25]$.

Effect of the Correlation Parameter ρ

The correlation ρ has a marked impact. Put-call parity improves with stronger leverage (up to 100% at $\rho = -0.8$), while smile convexity improves significantly with weaker correlation. Skew negativity and skew increase are satisfied in all cases for negative ρ but not for $\rho = 0$. The power-law fit is highest for strong negative correlation. Best results occur for $\rho \in [-0.6, -0.2]$.

Effect of the Volatility Scale Parameter a

The scale parameter a has a pronounced effect. For $a \leq 1.4$, most criteria exceed 80% success. At $a = 2.0$, performance collapses: smile convexity drops to 2%, put-call parity to 70%, and the power-law fit to 13%. This suggests a should be kept below 1.4, with optimal results for $a \in [0.7, 1.0]$.

Effect of the Base Volatility Level b

The base level b primarily shifts the surface level. Higher b improves smile convexity (52% at $b = 0.10$ to 72% at $b = 0.30$) and slightly supports skew criteria but reduces put-call parity (98% to 88%). Best balance occurs for $b \in [0.20, 0.30]$.

5.4 Optimal Parameter Ranges

The success rate analysis makes it possible to identify parameter regions that lead to stable and realistic implied volatility surfaces. Among all parameters, the roughness index H plays a central role. The best results are obtained for H between 0.10 and 0.25. In this range, put-call parity is fulfilled, smile convexity is more likely to hold, and the ATM skew follows a power law with good accuracy. For higher values of H, the power-law behavior deteriorates.

The persistence parameter γ_2 shows no strong sensitivity in the tested range. The model remains robust with respect to this parameter, and performance is broadly stable across all values. Slightly better results are obtained for smaller values, but the effect is minor compared to the influence of H or a.

The correlation parameter ρ has a more pronounced impact. Surfaces are most realistic when ρ lies between -0.6 and -0.2. Stronger negative correlations improve put-call parity and enhance the power-law fit, but at the same time reduce smile convexity. If ρ approaches zero, the ATM skew criterion is frequently violated, which is inconsistent with market data.

The volatility scale parameter a is critical for stability. For $a \leq 1.4$, most criteria are satisfied with high probability. Once a reaches 2.0, results collapse: smiles become non-convex, parity is often violated, and the power-law fit deteriorates sharply. Within the stable region, the best performance is observed for a between 0.7 and 1.0.

The base volatility level b mainly shifts the overall surface upward. Higher values improve smile convexity and the skew behavior, but reduce the accuracy of put-call parity. A balanced choice is obtained for b between 0.20 and 0.30, where all criteria perform well simultaneously.

In summary, the ranges $H \in [0.10, 0.25]$, $\rho \in [-0.6, -0.2]$, $a \in [0.7, 1.0]$, and $b \in [0.20, 0.30]$ provide the most robust performance. The persistence parameter γ_2 can be chosen flexibly, as the model is relatively insensitive to it. These ranges form a practical starting point for calibration to market data in Section 6.

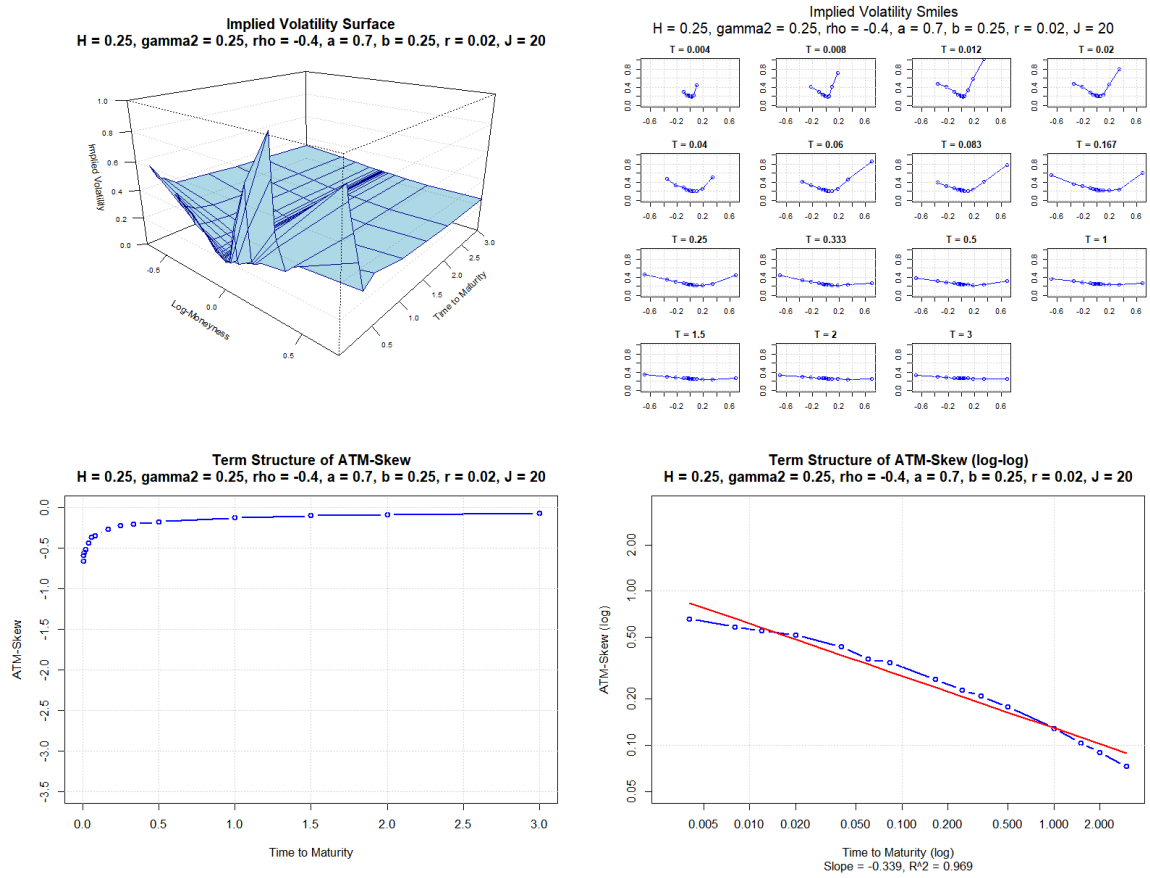

Figure 8: Example implied volatility surface, smiles, ATM skew, and log-log skew term structure for an optimal parameter configuration.

Figure 8 illustrates a surface generated with $H = 0.25$, $\gamma_2 = 0.25$, $\rho = -0.4$, $a = 0.7$, $b = 0.25$, $r = 0.02$, and $J = 20$ (with γ_1 set according to Equation (10)). This configuration satisfies all five criteria and produces a surface shape consistent with empirical market data.

6 Empirical Validation

This section provides an empirical validation of the Hypergeometric Volatility Model by comparing simulated implied volatility surfaces with observed market data. The analysis is based on S&P 500 option data from the OptionMetrics database (accessed via WRDS) for March 2023.

A mean implied volatility surface is constructed on a fixed moneyness-maturity grid using linear interpolation to ensure comparability with the simulated surfaces. The evaluation proceeds in two steps. First, the simulation quality criteria from Section 5.1 are tested on the empirical surface. Second, the model is calibrated by identifying the parameter configuration that yields the closest fit to the market surface, measured by the Mean Squared Error (MSE).

6.1 Empirical Volatility Surface

Data Collection and Preparation

S&P 500 option data for March 2023 were obtained from the OptionMetrics database via WRDS. The dataset includes implied volatilities, strike prices, and expiration dates for listed equity index options.

Data cleaning was performed to remove extreme or invalid entries. Excluded were:

- Implied volatilities above 100%,
- Maturities longer than three years,
- Extremely deep in- or out-of-the-money options.

After cleaning, the dataset contained approximately 373,000 observations from March 1 to March 31, 2023. Maturities range from 1 day to 3 years, and strikes cover a wide range of moneyness values from $K/S = 0.3$ to $K/S = 3.1$. This provides a broad cross-section of the implied volatility surface across both short and long maturities.

Strike prices were converted to moneyness using the ratio K/S, and maturities were expressed in years. The data were binned onto a discrete moneyness-maturity grid, averaged within bins, and interpolated linearly. The resulting surface was evaluated on the same grid used in Section 5, consisting of 17 moneyness levels

$$\{0.5,\ 0.7,\ 0.8,\ 0.9,\ 0.95,\ 0.975,\ 0.99,\ 0.995,\ 1,\ 1.005,\ 1.01,\ 1.025,\ 1.05,\ 1.1,\ 1.2,\ 1.4,\ 2\}$$

and 15 maturities (in trading days)

$$\{1,\ 2,\ 3,\ 5,\ 10,\ 15,\ 21,\ 42,\ 63,\ 84,\ 126,\ 252,\ 378,\ 504,\ 756\},$$

assuming 252 trading days per year. This grid yields 255 evaluation points at which empirical and simulated implied volatilities are compared directly, so that no additional interpolation is required during calibration.

Evaluation of Quality Criteria

The empirical surface satisfies all four simulation quality criteria that can be evaluated based on implied volatilities. The put-call parity criterion cannot be tested, since OptionMetrics provides implied

volatilities but not raw option prices.

Figure 9 and the associated diagnostics (volatility smiles, ATM skew, and log-log ATM skew term structure) confirm that the empirical surface exhibits the key stylized facts observed in financial markets: convex volatility smiles, a negative at-the-money skew, an increasing skew term structure, and approximate power-law decay. The regression on the log-log plot of the ATM skew against maturity achieves an R^2 value of 95.5%, with an estimated decay exponent of $\gamma = 0.291$. Following Fukasawa (2011), this corresponds to an implied roughness parameter of $H = \frac{1}{2} - \gamma = 0.209$. These findings demonstrate that the empirical S&P 500 surface is consistent with the quality criteria introduced in Section 5.1, and thus provide a suitable benchmark for the calibration of the Hypergeometric Volatility Model.

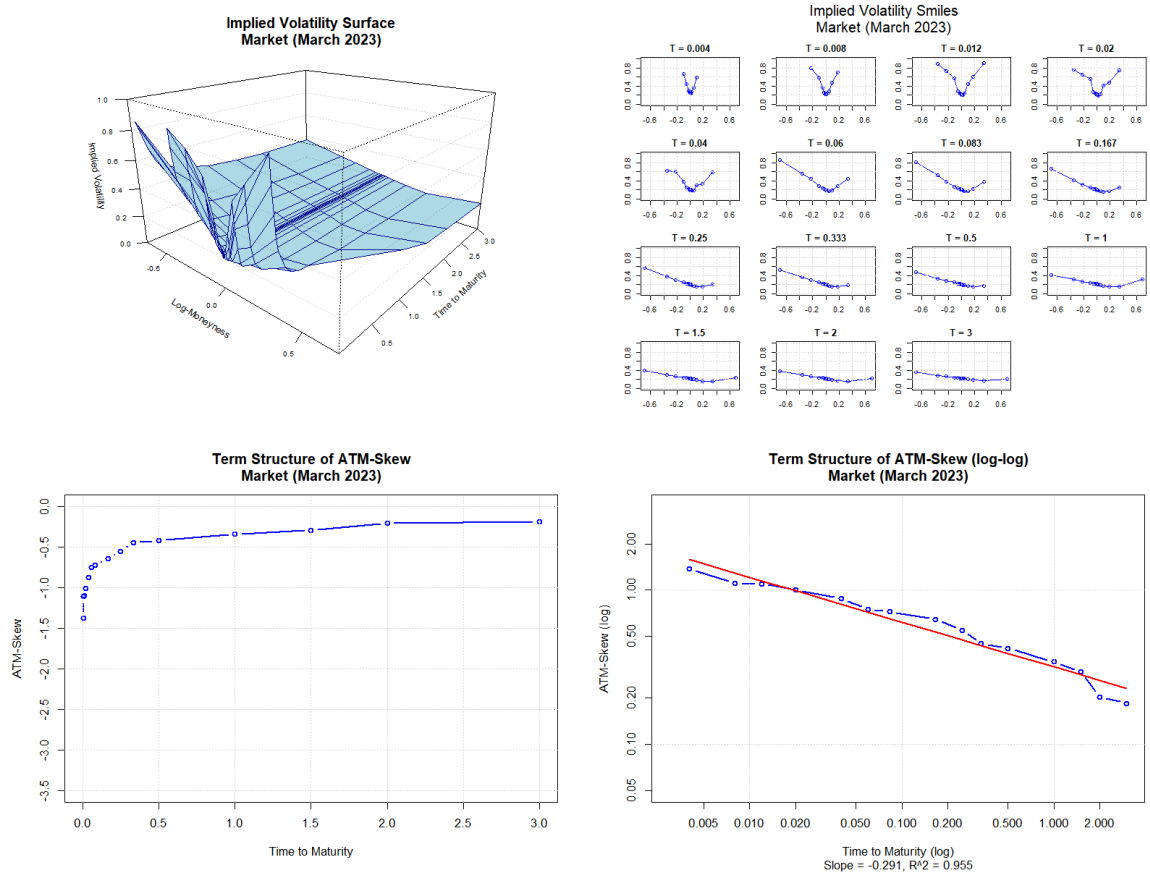

Figure 9: Empirical implied volatility surface, volatility smiles, ATM skew, and log-log skew term structure (S&P 500; March 2023).

6.2 Calibration to Market Data

Calibration Methodology

The calibration was performed using a grid search approach. All 18,225 parameter configurations from the simulation study in Section 5.3 were evaluated through comparison of their simulated volatility surfaces with the empirical market surface from Section 6.1. For each scenario, the goodness of fit was assessed by the Mean Squared Error (MSE) computed over the predefined strikes-maturities

grid:

$$\text{MSE} = \frac{1}{N} \sum_{i=1}^{N} \left(\sigma_{\text{model}}^{(i)} - \sigma_{\text{market}}^{(i)} \right)^2, \tag{34}$$

where $\sigma_{\text{model}}^{(i)}$ and $\sigma_{\text{market}}^{(i)}$ denote the model-implied and market-implied volatilities at grid point i, and N is the total number of grid points with valid data. The parameter set yielding the lowest MSE was identified as the best fit to the market surface.

Best Fit Parameter Set

The configuration minimizing the MSE is

$$\{H = 0.05, \quad \gamma_2 = 0.20, \quad \rho = -0.7, \quad a = 1.0, \quad b = 0.20, \quad r = 0.02, \quad J = 20\}.$$

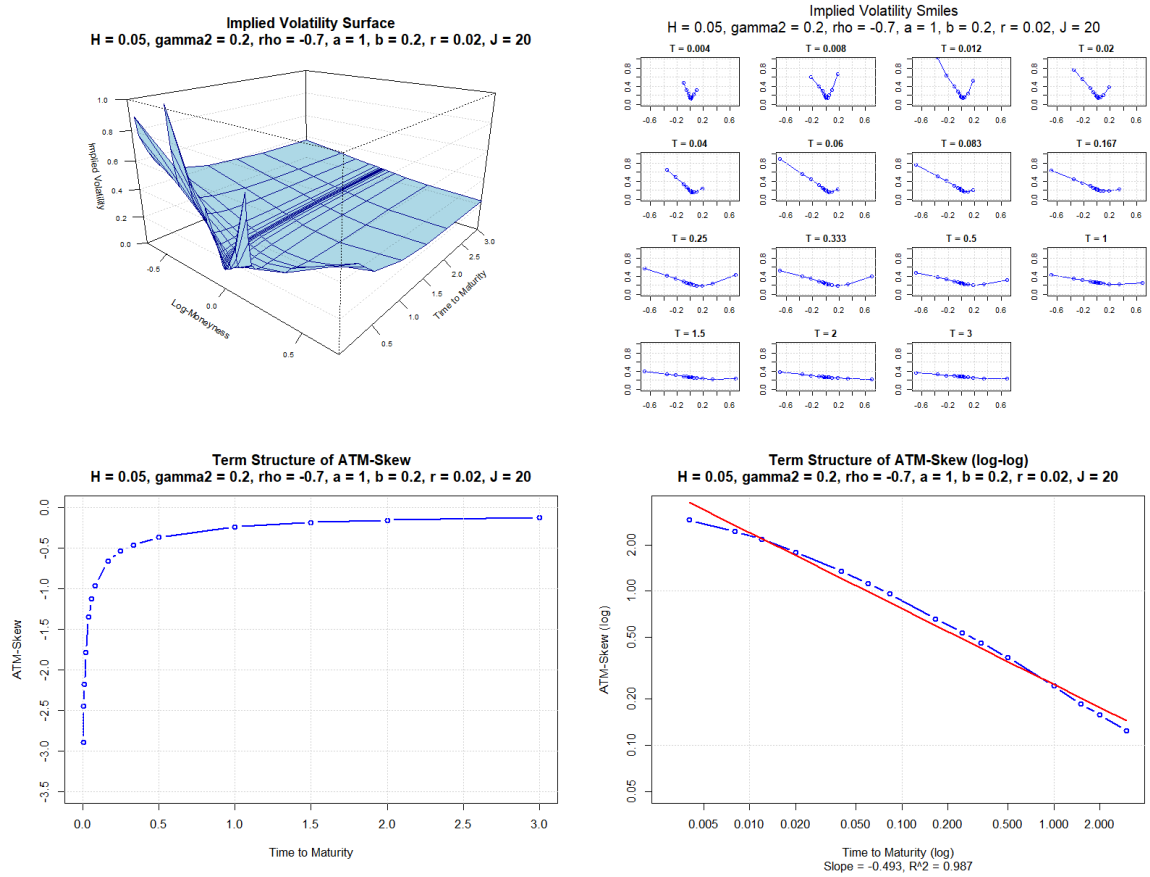

Figure 10: Calibrated implied volatility surface, smile slices, ATM skew, and log-log skew term structure.

The calibrated surface in Figure 10 reproduces the key characteristics of the S&P 500 volatility surface. The overall shape of the volatility smiles, the negative and increasing ATM skew, and the approximate power-law decay are all matched with high accuracy. The strongest agreement is observed in the short-maturity and near-the-money region, where option prices are most liquid and reliable.

These results confirm that the Hypergeometric Volatility Model is capable of replicating essential stylized features of market volatility surfaces, provided that parameter values remain within the favorable ranges identified in Section 5.3.

7 Conclusion

This thesis examined the Hypergeometric Volatility Model as a framework for reproducing key features of implied volatility surfaces observed in financial markets. A broad simulation study, combined with empirical validation using S&P 500 option data, was conducted to evaluate the model's ability to match empirical stylized facts and to determine parameter settings that generate realistic surfaces.

To assess how realistic simulated surfaces are, five quality criteria were established: put-call parity, smile convexity, negative at-the-money (ATM) skew, increasing skew term structure, and approximate power-law decay. More than 18,000 parameter combinations were simulated to analyze the effect of roughness, persistence, correlation, and volatility scaling on the implied volatility surface. The results identified key parameter ranges for optimal model performance: roughness indices H between 0.10 and 0.25, correlation parameters ρ in the range $[-0.6, -0.2]$, and volatility scale values a below 1.4. The persistence parameter γ_2 showed relatively modest effects, although slightly better performance was observed for smaller values. While roughness, correlation, and volatility scale showed the strongest effects, the choice of base volatility also contributed to surface realism.

Across all parameter constellations, the overall success rate of scenarios that satisfied all five criteria was 54%. Put-call parity and negative skew were satisfied in most cases (93% and 99%, respectively), while smile convexity was harder to achieve, with a success rate of 66%. This analysis offers practical guidance for the implementation of the Hypergeometric Volatility Model by identifying parameter regions that consistently produce market-realistic outcomes.

The empirical validation confirmed that the model was able to reproduce essential features of the S&P 500 volatility surface, particularly in near-the-money and short-maturity regions. However, an interesting discrepancy was observed in the calibration results: the best-fit parameter configuration yielded $H = 0.05$ and $\rho = -0.7$, which fell just outside the optimal ranges identified in the simulation study. Nevertheless, their corresponding success rates remained high and only slightly below those observed in the optimal regions. This shows that parameter regions that perform well in terms of stylized facts may not coincide with those that best fit market data. The calibrated roughness parameter also differed from the theoretical roughness of $H \approx 0.21$ implied by the power-law decay observed in the empirical surface, which highlights the difficulty of linking empirical observations to model parameters. In contrast, the volatility scale $a = 1.0$ and base volatility $b = 0.20$ from the best-fit configuration matched the expected ranges well.

The findings highlight both the strengths and the limitations of the Hypergeometric Volatility Model. On the positive side, the model provides a flexible framework capable of generating rough volatility effects and empirically consistent skew behavior through explicit control of roughness and persistence parameters. The model reproduces key stylized facts when appropriately parameterized and remains computationally feasible through finite-dimensional approximations. Limitations arise in the trade-off between achieving high success across all criteria and obtaining the best fit to market data, as well as in numerical stability at extreme parameter values.

A number of open questions remain that could be addressed in future work. The discrepancy between simulation-optimal and calibration-optimal parameters suggests the need for calibration methods that balance fit quality with stylized fact reproduction, possibly through multi-objective optimization approaches. The current calibration was performed using a grid search approach over the strike-

maturity grid, which has higher concentration of data points for shorter maturities and for at-the-money strikes. More advanced calibration methods, such as derivative-free optimization, could be used to navigate the parameter space more efficiently and to search for configurations that reconcile robustness with market fit. In addition, systematic comparisons with alternative rough volatility models could provide a clearer view of the model's relative strengths and weaknesses.

In summary, this thesis has shown that the Hypergeometric Volatility Model is able to reproduce central empirical features of option markets, while also revealing important aspects in the relationship between parameter selection and model performance. The parameter analysis provides useful guidance for practical implementation, but the calibration results emphasize that real-world applications require careful handling of trade-offs between competing modeling objectives. With further methodological refinements and broader empirical testing, the model has the potential to become a valuable tool in both academic research and financial practice.

A Figures

A.1 Process Dynamics Illustration

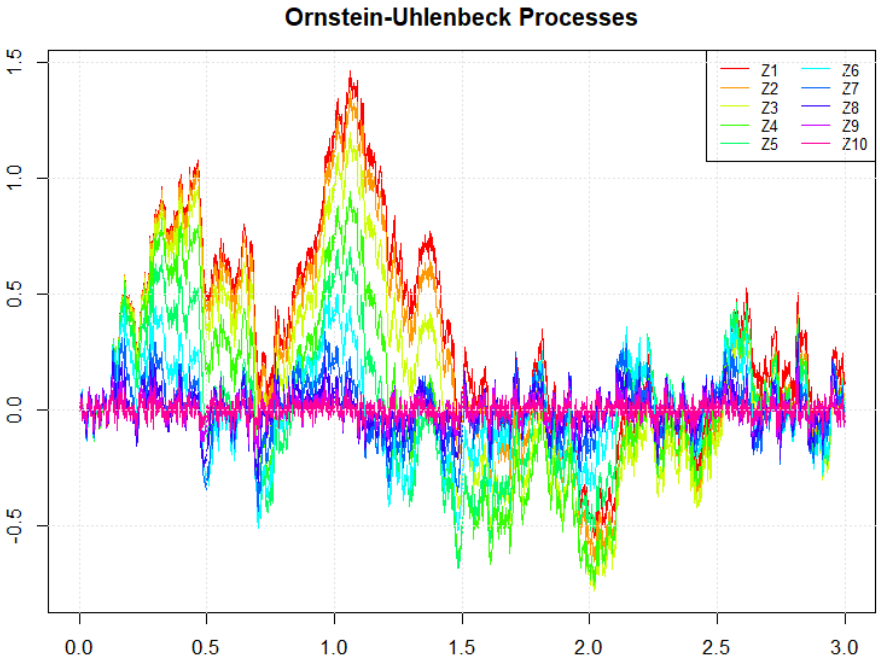

Figure 11: Sample Ornstein-Uhlenbeck processes with different mean-reversion speeds.

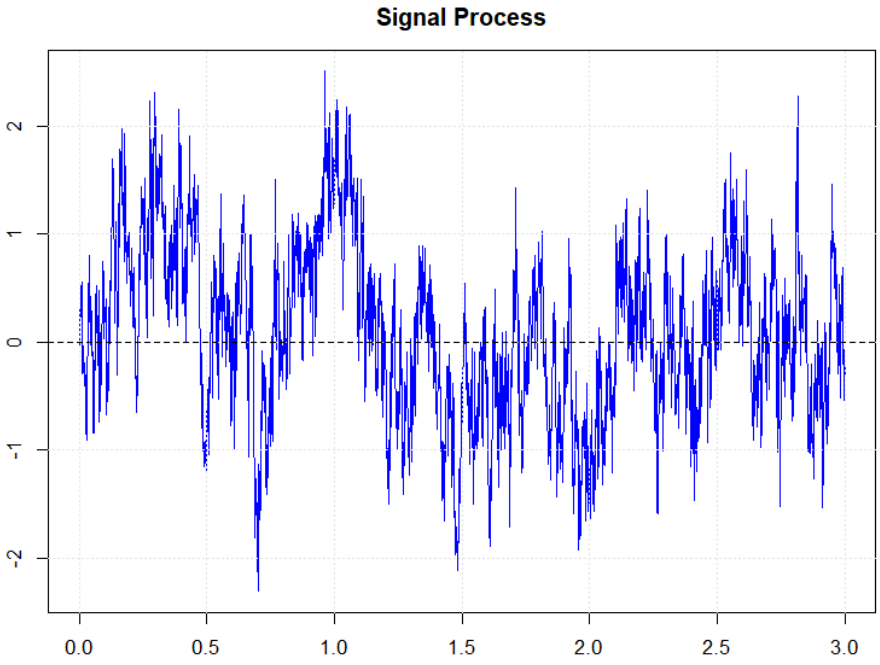

Figure 12: Signal process obtained as a weighted combination of OU processes. The aggregation produces rough and persistent sample paths, consistent with empirical volatility dynamics.

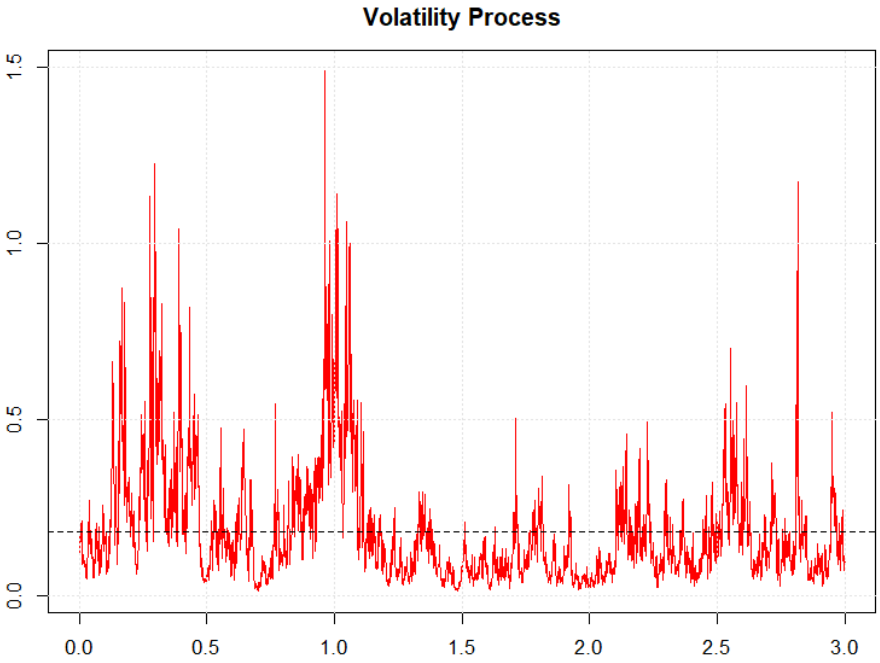

Figure 13: Volatility process derived via exponential transformation of the signal. The process remains strictly positive and exhibits clustering and occasional spikes.

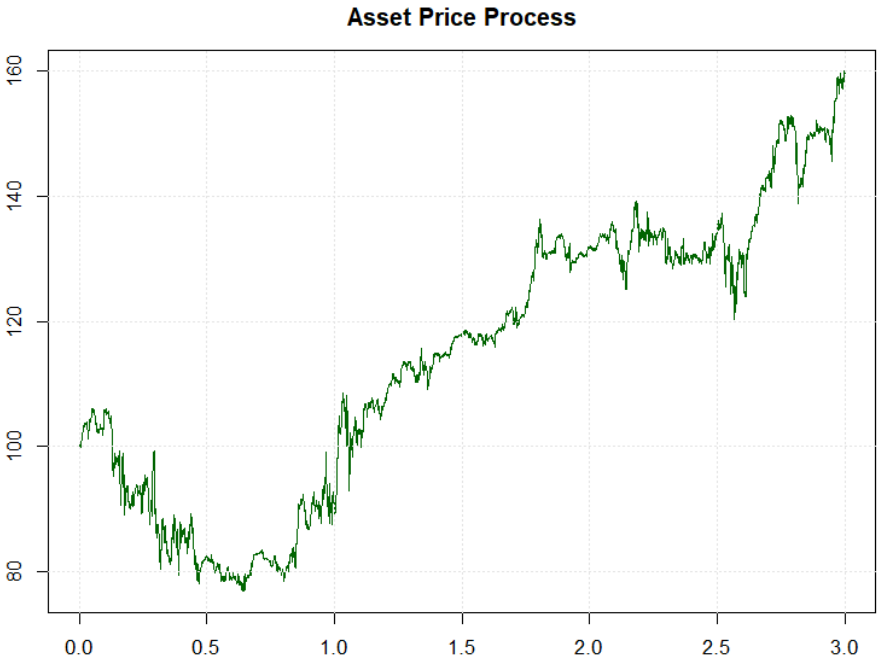

Figure 14: Simulated asset price process driven by the stochastic volatility. The trajectory reflects both drift and volatility clustering effects.

A.2 Additional Market Surface

To illustrate the stability of the empirical implied volatility surface across different sample periods, Figure 15 shows the S&P 500 surface constructed from April 2023 option data. The same cleaning and interpolation procedures as described in Section 6.1 were applied. The surface exhibits the same qualitative features as the March 2023 surface: convex volatility smiles, a negative and increasing ATM skew, and an approximate power-law decay in the skew term structure. This confirms that the stylized facts underlying the simulation quality criteria are consistently present in market data across different months.

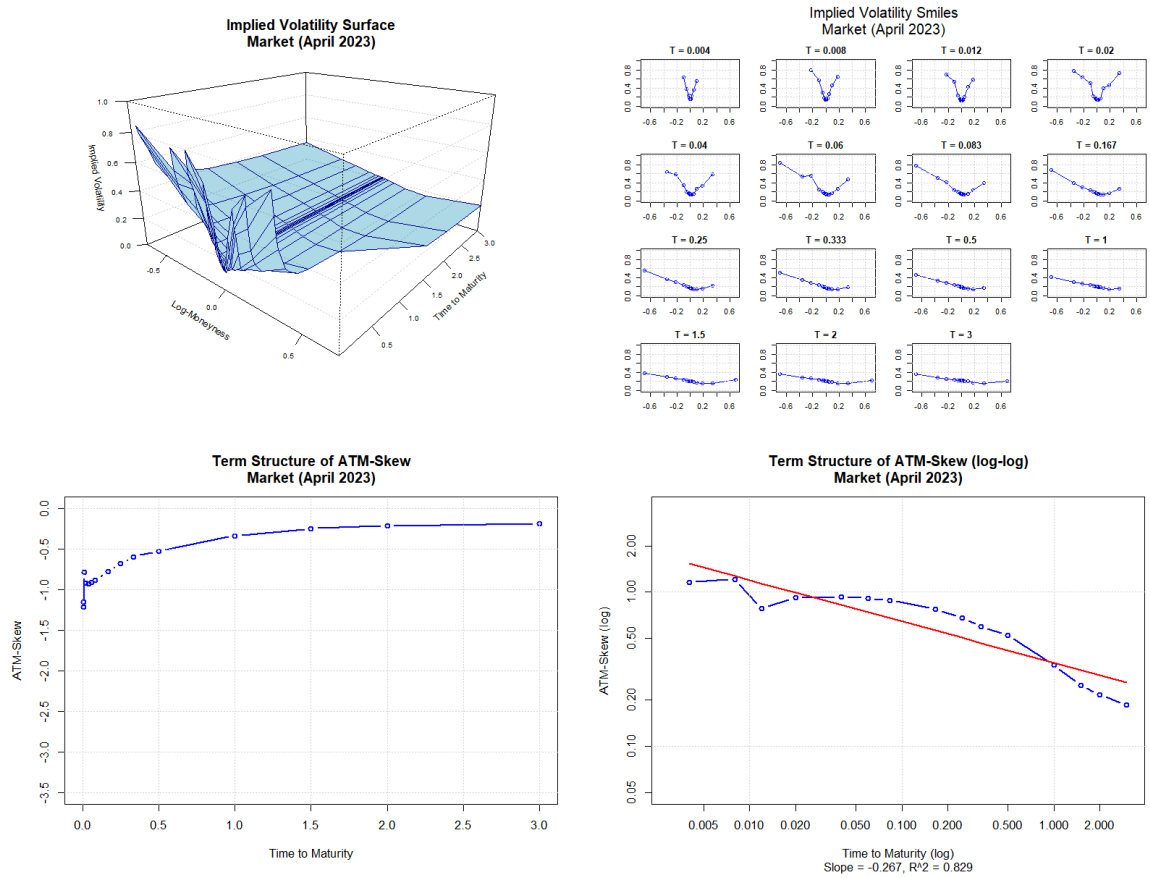

Figure 15: Empirical implied volatility surface, volatility smiles, and ATM skew (S&P 500; April 2023).

A.3 Calibration Diagnostics

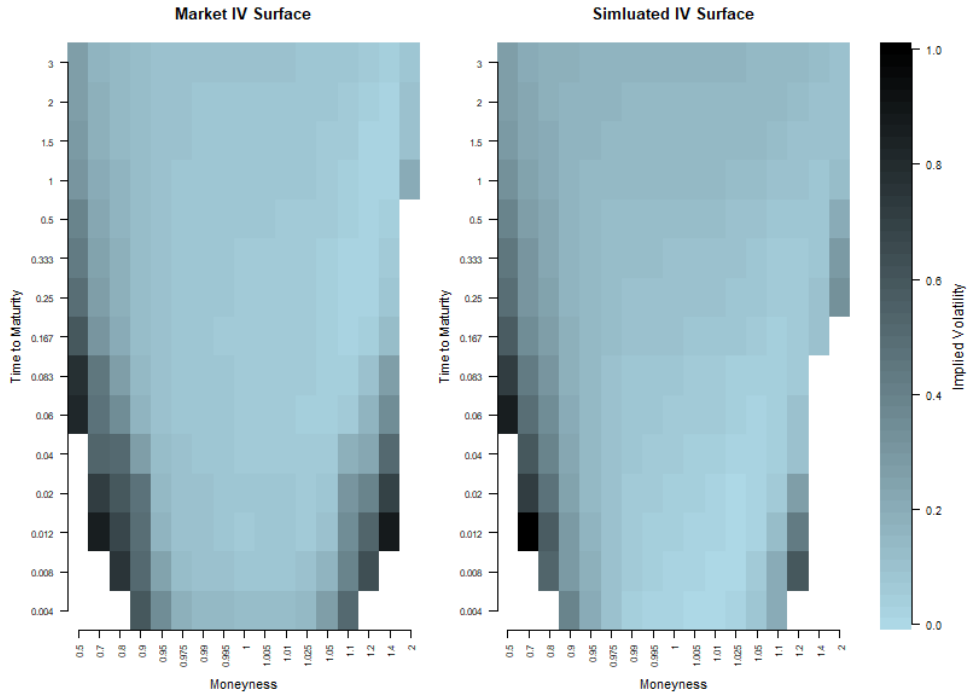

Figure 16: Heatmap comparison of the empirical implied volatility surface (S&P 500, March 2023) and the calibrated Hypergeometric Volatility Model surface.

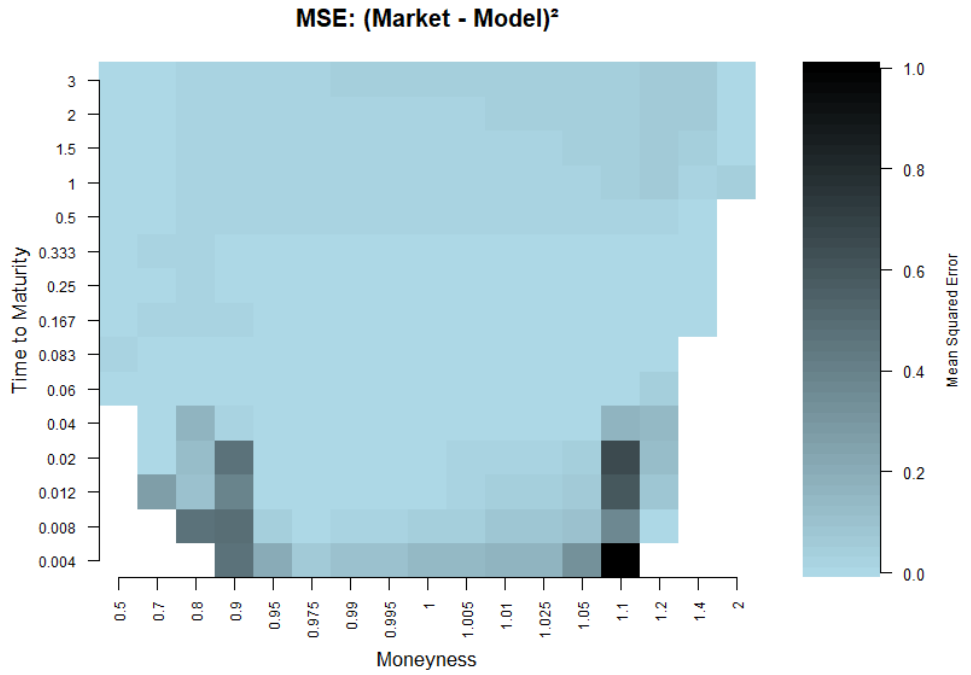

Figure 17: Heatmap of the squared error between the empirical and calibrated implied volatility surfaces. Errors are concentrated in short-maturity and far out-of-the-money regions, highlighting areas where the model struggles to capture market dynamics.

B Tables

B.1 Success Rate Analysis Results

Parameter	Put-Call Parity	Smile Convexity	Skew Negative	Skew Increasing	Skew Power Law	All
			H			
0.05	84%	67%	99%	100%	77%	58%
0.10	87%	71%	99%	100%	76%	60%
0.15	90%	71%	100%	100%	74%	61%
0.20	92%	69%	100%	99%	73%	60%
0.25	94%	69%	99%	97%	73%	59%
0.30	96%	66%	99%	95%	71%	56%
0.35	97%	63%	99%	93%	69%	51%
0.40	98%	60%	99%	91%	65%	45%
0.45	99%	58%	99%	90%	57%	38%
			γ_2			
0.05	90%	67%	99%	98%	70%	55%
0.10	91%	67%	99%	97%	70%	55%
0.15	92%	66%	99%	97%	70%	55%
0.20	92%	66%	99%	96%	70%	55%
0.25	93%	66%	99%	96%	71%	55%
0.30	94%	66%	99%	96%	70%	54%
0.35	95%	66%	99%	95%	71%	54%
0.40	96%	65%	99%	95%	71%	53%
0.45	96%	64%	99%	95%	71%	52%
			ρ			
−0.8	100%	11%	100%	100%	85%	11%
−0.7	100%	57%	100%	100%	85%	57%
−0.6	98%	73%	100%	100%	84%	73%
−0.5	97%	75%	100%	100%	83%	73%
−0.4	95%	74%	100%	100%	82%	74%
−0.3	92%	74%	100%	100%	80%	73%
−0.2	89%	75%	100%	100%	76%	72%
−0.1	86%	76%	100%	100%	58%	55%
0.0	82%	77%	93%	65%	0%	0%
			a			
0.5	100%	85%	97%	99%	83%	68%
0.7	100%	84%	99%	96%	86%	70%
1.0	100%	83%	100%	95%	87%	71%
1.4	96%	75%	100%	95%	83%	61%
2.0	70%	2%	100%	96%	13%	1%
			b			
0.10	98%	52%	100%	95%	66%	42%
0.15	96%	65%	100%	96%	68%	54%
0.20	93%	69%	100%	96%	69%	58%
0.25	91%	71%	99%	97%	72%	58%
0.30	88%	72%	97%	97%	77%	58%
			r			
0.02	93%	66%	99%	96%	70%	54%
			J			
20	93%	66%	99%	96%	70%	54%

Table 2: Success Rates Across Parameter Values

B.2 Optimal Parameter Ranges

Parameter	Optimal Range	Notes
Roughness index H	$[0.10, 0.25]$	Best trade-off across criteria
Persistence γ_2	Stable across $[0.05, 0.45]$	Slightly better for smaller values
Correlation ρ	$[-0.6, -0.2]$	Negative correlation required
Volatility scale a	$[0.7, 1.0]$	Instability for $a > 1.4$
Base volatility b	$[0.20, 0.30]$	Higher b improves convexity

Table 3: Optimal parameter ranges identified in the simulation study (Section 5.3).

C References

Eduardo Abi Jaber, Martin Larsson, and Sergio Pulido. Affine Volterra processes. *The Annals of Applied Probability*, 29(5):3155–3200, 2019.

Christian Bayer, Peter Friz, and Jim Gatheral. Pricing under rough volatility. *Quantitative Finance*, 16 (6):887–904, 2016.

Mikkel Bennedsen, Asger Lunde, and Mikko S. Pakkanen. Decoupling the short- and long-term behavior of stochastic volatility. *Journal of Financial Econometrics*, 19(2):301–328, 2021.

Tomas Björk. *Arbitrage Theory in Continuous Time*. Oxford University Press, 3rd edition, 2009.

Fischer Black and Myron Scholes. The pricing of options and corporate liabilities. *Journal of Political Economy*, 81(3):637–654, 1973.

Philippe Carmona and Laure Coutin. Fractional Brownian Motion and the Markov Property. *Electronic Communications in Probability*, 3(none):95–107, 1998.

Philippe Carmona, Laure Coutin, and Gérard Montseny. Approximation of some gaussian processes. *Statistical Inference for Stochastic Processes*, 3:161–171, 2000.

Fabienne Comte and Eric Renault. Long memory in continuous-time stochastic volatility models. *Mathematical Finance*, 8(4):291–323, 1998.

Rama Cont. Empirical properties of asset returns: Stylized facts and statistical issues. *Quantitative Finance*, 1(2):223–236, 2001.

Camilla Damian. *Statistical Inference for Partial Information Models in Finance: Three Essays*. Phd thesis, Vienna University of Economics and Business, Vienna, 2021. URL `https://permalink.obvsg.at/wuw/AC16426351`.

Camilla Damian and Rüdiger Frey. Detecting rough volatility: a filtering approach. *Quantitative Finance*, 24(10):1493–1508, 2024.

Omar El Euch and Mathieu Rosenbaum. The characteristic function of rough heston models. *Mathematical Finance*, 29(1):3–38, 2019.

Masaaki Fukasawa. Asymptotic analysis for stochastic volatility: Edgeworth expansion. *Electronic Journal of Probability*, 16:764–791, 2011.

Masaaki Fukasawa. Short-time at-the-money skew and rough fractional volatility. *Quantitative Finance*, 17(2):189–198, 2017.

Jim Gatheral, Thibault Jaisson, and Mathieu Rosenbaum. Volatility is rough. *Quantitative Finance*, 18(6):933–949, 2018.

Steven L. Heston. A closed-form solution for options with stochastic volatility with applications to bond and currency options. *The Review of Financial Studies*, 6(2):327–343, 1993.

Mark Rubinstein. Nonparametric tests of alternative option pricing models using all reported trades

and quotes on the 30 most active cboe option classes from august 23, 1976 through august 31, 1978. *The Journal of Finance*, 40(2):455–480, 1985.